Electron-impact ionization of Bi^{q+} for $q=1-10$

S. D. Loch and M. S. Pindzola
Department of Physics, Auburn University, Auburn, Alabama 36849, USA

N. R. Badnell
Department of Physics, University of Strathclyde, Glasgow, G4 0NG, United Kingdom

F. Scheuermann, K. Kramer, K. Huber, and E. Salzborn
Institut für Kernphysik, University of Giessen, D-35392 Giessen, Germany
(Received 11 May 2004; published 24 November 2004)

Theoretical calculations and experimental crossed-beam measurements are compared for electron-impact single ionization of Bi^{q+} for $q=1-10$. The configuration-average distorted-wave calculations include both direct ionization and indirect excitation-autoionization contributions. For Bi^{2+} it is necessary to account for levels within an excited configuration that straddle the ionization threshold. This was included via level-resolved atomic structure calculations, from which statistical partitions of the configuration-averaged cross sections could then be made. Evidence is found for ionization contributions from an excited configuration in Bi^{3+} and Bi^{5+}. Good agreement is found between theory and experiment for all the ionization stages of Bi studied.

DOI: 10.1103/PhysRevA.70.052714 PACS number(s): 34.80.Dp, 52.20.Fs

I. INTRODUCTION

For the next generation of magnetically confined fusion experiments, heavy metals are being considered for plasma facing components due to their ability to withstand high heat loads and erosion [1,2]. Accurate electron-impact excitation, ionization, and recombination rates for heavy metals are needed to model the transport of the resultant impurity ions in present day tokamak experiments. Even for electron-impact ionization rates it is possible for atomic experiments to measure only a limited number of elements and their ionization stages. Thus, it is important to check theory against experiments for all heavy metals. We present a comparison between crossed-beam measurements and distorted-wave theory for the ionization cross section of Bi^{+} through to Bi^{10+}.

The configuration-average distorted-wave (CADW) method [3] was formulated to calculate electron impact excitation, ionization, and recombination cross sections for complex atomic ions. The CADW method was initially applied to calculate electron-impact ionization cross sections for all ionization stages of Fe [4,5] and Ni [6,7]. Since that time, both CADW calculations and experimental crossed-beam measurements have been carried out for the electron-impact ionization of several elements heavier than Fe, including Ga^{q+} ($q=1-9$) [8], Mo^{q+} ($q=1-8$) [9], Sm^{q+} ($q=1-12$) [10], and W^{q+} ($q=1-10$) [11,12]. Recently, CADW calculations have been completed for the electron-impact ionization of all ionization stages of Kr [13], while work is in progress for all ionization stages of W [14].

We compare our CADW results with those of the Lotz expression [16]. The Lotz expression is a semiempirical method, where the total ionization cross section (cm^2) from subshells k with occupation number ξ_k, ionization potential I_k (eV), as a function of incident electron energy ε (eV), is given by

$$\sigma(\varepsilon) = 4.5 \times 10^{-14} \sum_k \xi_k \frac{\ln(\varepsilon/I_k)}{\varepsilon I_k}. \quad (1)$$

In this paper we apply the CADW method to calculate electron-impact ionization cross sections for Bi^{q+} ($q=1-10$) to compare with experimental crossed-beam measurements. Previous experimental measurements on the single and double ionization cross sections for Bi^{+} and Bi^{2+} were performed by Müller *et al.* [15]. They found that for Bi^{+}, inner shell ionization of the 5*d* subshell left the system in a configuration that was autoionizing. Thus direct ionization of the 5*d* subshell leads to a double ionization of Bi^{+}. In contrast, for Bi^{2+}, ionization of the 5*d* subshell leaves the system in a configuration that is bound. For this reason, at energies above 200 eV, the single ionization cross section for Bi^{2+} was measured to be greater than the cross section for Bi^{+}. To our knowledge, no experimental measurements have been published on electron-impact single ionization of Bi^{3+} through to Bi^{10+}.

There have been very few theoretical calculations of the single ionization cross section of low charged Bi ions. As part of the work on Bi^{+} and Bi^{2+} by Müller *et al.* [15], Lotz formula [16] calculations were performed. The Lotz calculations demonstrated the behavior of the 5*d* inner shell ionization, but did not match the experimental measurements because of contributions from excitation-autoionization. To the best of our knowledge, no theoretical calculations have been published for the remaining ion stages of Bi. In Sec. II we outline the theory used in the paper, Sec. III describes the experimental setup, Sec. IV compares the experimental and theoretical results, and in Sec. V we summarize our results.

II. THEORY

The main contributions to the electron-impact single ionization cross section are from direct ionization

$$\mathrm{Bi}^{q+} + e^- \rightarrow \mathrm{Bi}^{(q+1)+} + e^- + e^-, \tag{2}$$

and excitation-autoionization

$$\mathrm{Bi}^{q+} + e^- \rightarrow (\mathrm{Bi}^{q+})^* + e^- \rightarrow \mathrm{Bi}^{(q+1)+} + e^- + e^-. \tag{3}$$

Here q is the initial charge of the ion, $(\mathrm{Bi}^{q+})^*$ represents an excited state of the ion, and for the process of excitation-autoionization, there is also the possibility of radiative stabilization occurring before the excited ion can autoionize. Thus, autoionization configurations are associated with an Auger yield, giving the fraction of electrons that will autoionize from such a configuration.

We present theoretical results using configuration-average distorted-wave theory [3]. In this approach, the cross section for single ionization of an electron from the $(n_t l_t)^{\omega_t}$ subshell is given by

$$\sigma = \frac{32\omega_t}{k_i^3}\int_0^{E/2}\frac{d(k_e^2/2)}{k_e k_f}\sum_{l_i,l_e,l_f}(2l_i+1)(2l_e+1) \times(2l_f+1)P(l_i,l_e,l_f,k_i,k_e,k_f), \tag{4}$$

where the linear momenta (k_i,k_e,k_f) and the angular momentum quantum numbers (l_i,l_e,l_f) correspond to the incoming, ejected, and outgoing electron, respectively. The first order scattering probability is given by

$$\begin{aligned}P(l_i,l_e,l_f,k_i,k_e,k_f) = &\sum_{\lambda} A^{\lambda}_{l_i,l_e,l_f}[R^{\lambda}(k_e l_e,k_f l_f,n_t l_t,k_i l_i)]^2 \\ &+ \sum_{\lambda'} B^{\lambda'}_{l_i,l_e,l_f}[R^{\lambda'}(k_f l_f,k_e l_e,n_t l_t,k_i l_i)]^2 \\ &+ \sum_{\lambda}\sum_{\lambda'} C^{\lambda,\lambda'}_{l_i,l_e,l_f} R^{\lambda}(k_e l_e,k_f l_f,n_t l_t,k_i l_i) \\ &\times R^{\lambda'}(k_f l_f,k_e l_e,n_t l_t,k_i l_i),\end{aligned} \tag{5}$$

where the angular coefficients A, B, C may be expressed in terms of standard 3-j and 6-j symbols and R^{λ} are standard Slater integrals. The radial distorted waves $P_{kl}(r)$ needed to evaluate the Slater integrals are solutions to a radial Schrödinger equation given by

$$\left(h(r) - \frac{k^2}{2}\right)P_{kl}(r) = 0, \tag{6}$$

where

$$h(r) = -\frac{1}{2}\frac{d^2}{dr^2} + \frac{l(l+1)}{2r^2} - \frac{Z}{r} + V_D(r) + V_X(r), \tag{7}$$

and Z is the atomic number. The direct potential is given by

$$V_D(r) = \sum_u^{occ}\omega_u\int_0^{\infty}\frac{P^2_{n_u l_u}(r')}{max(r',r)}dr', \tag{8}$$

where $P_{n_u l_u}(r)$ are the configuration-average Hartree-Fock bound radial orbitals. The exchange potential is calculated in a local density approximation. There are commonly two different approximations made for the scattering potential that the incident, scattered, and ejected electrons experience. The incident and scattered electrons can be evaluated in a V^N potential, with the ejected continuum electron calculated in a V^{N-1} potential, where N is the number of electrons in the initial target. This is referred to as the DWIS(N) (distorted-wave, incident, and scattered electron in a V^N potential). Alternatively one can calculate the incident, scattered, and ejected electrons in a V^{N-1} potential, labeled as DWIS($N-1$).

There are various refinements possible to improve a configuration-average distorted-wave calculation. It is occasionally the case that splitting of levels within an excited configuration results in a spread of levels which straddle the ionization threshold. The configuration-average model includes all the contributions from a configuration, or omits it, depending on whether the excitation threshold lies above or below the ionization potential. Thus, one possible refinement of the configuration-average distorted-wave method is to use a level-resolved structure calculation to determine which levels are truly autoionizing. Level-resolved excitation cross sections are then produced for each level by a statistical partition of the configuration-average excitation cross section. The level-resolved energies are used to determine the excitation thresholds for the level-resolved cross sections. All levels below the ionization threshold are omitted, and all the levels that lie above the threshold are considered contributors to the total cross section. Level-resolved Auger yields are used on the autoionizing levels such that the total excitation-autoionization cross section is produced. For cases where it is expected that straddling of the autoionization threshold is occurring the AUTOSTRUCTURE code [17–19] is used to evaluate the level-resolved atomic structure of the excited configurations, and the level-resolved Auger yields.

For complex species with open d and p shells, there will be many terms within the ground configuration. In such circumstances the configuration-average model should become a good representation of the average behavior of the configuration. Also, with so many terms within the ground configuration, one might expect any metastable terms to be included in the ground configuration. Thus, the configuration-average distorted-wave model should provide a reasonable calculation for the single ionization cross section of heavy species such as bismuth. Good agreement of configuration-average distorted-wave calculations with complex species has been seen numerous times in previous work, for example, in the work in krypton [13] or tungsten [12].

III. EXPERIMENTAL SETUP

The measurements were performed at the Giessen electron-ion crossed-beam setup which has been described in detail earlier (Tinschert *et al.* [20], Hofmann *et al.* [21]). The Bi^{q+} ions were produced by evaporating bismuth granulate from an oven into the plasma of our newly installed 14 GHz electron cyclotron resonance ion source (Brötz [22]). Using a magnetic field the desired mass to charge ratio was selected. After tight collimation to typically 1×1 mm^2 the ion beam

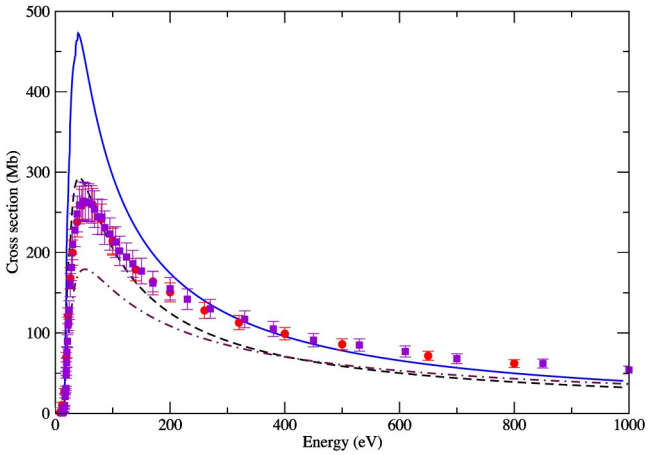

FIG. 1. Electron-impact single ionization cross section for Bi^+. The dashed line gives the total configuration-average distorted-wave direct ionization, and the solid line gives the total configuration-average distorted-wave direct plus the total configuration-average distorted-wave excitation-autoionization cross section. The dot-dashed line shows the Lotz direct ionization cross section. The solid circles show the current experimental measurements and the solid squares show the measurements of Müller *et al.* [15].

was crossed with an intense electron beam. After collimation we had about 20 nA current of Bi^{10+} ions; for lower charge states higher currents could be obtained. The acceleration voltage used is 10 kV. The ionization products were separated from the incident ion beam after the interaction using a magnetic field. They were detected by a single particle detector, while a large Faraday cup collected the primary ion beam.

In the dynamic crossed-beam technique (Müller *et al.* [15]) the electron gun is moved up and down across the ion beam with simultaneous registration of the ionization signal. The electron and the ion currents were used to obtain the absolute cross sections. The electron gun was designed by Becker *et al.* [23] and delivers an electron current of 430 mA at the maximum energy of 1 keV. The typical measurement time is about 40 s for large cross sections at high energies and up to 2000 s near threshold. The total experimental uncertainties of the measured cross sections are typically 8% at the maximum, resulting from the quadrature sum of the nonstatistical errors of about 7.8% and the statistical error at 95% confidence level.

IV. RESULTS

A. Bi^+

The theoretical and experimental results for Bi^+ are shown in Fig. 1. Bi^+ has a ground configuration of $5d^{10}6s^26p^2$. The configuration-average results show the direct ionization of the 6*p* and 6*s* subshells. The direct ionization of the 5*d* subshell leads to a double ionization, as was reported previously by Müller *et al.* [15], and is not included in the calculation. Note that the current experimental measurements are in good agreement with the previous values of Müller *et al.* [15].

TABLE I. Configuration-average ionization potentials for the subshells in the ground configuration of Bi^+; the configuration-average double ionization potential is 39.41 eV.

Transition	Configuration-average ionization potential (eV)
$5d^{10}6s^26p^2 \rightarrow 5d^{10}6s^26p^1$	15.57
$5d^{10}6s^26p^2 \rightarrow 5d^{10}6s^16p^2$	26.22
$5d^{10}6s^26p^2 \rightarrow 5d^96s^26p^2$	43.22

Table I shows the direct ionization potentials for Bi^+. We also include the effects of excitation-autoionization via the $5d^96s^26p^2nl$ and $5d^{10}6s^16p^2nl$ configurations, where $n=5-8$ and $l=0-3$. The results from the direct ionization are reasonably close to experiment; however, once excitation-autoionization is accounted for, the CADW results are significantly higher than experiment. The distorted-wave calculation is overestimating the cross section for such a near neutral species, a not uncommon occurrence. The total Lotz cross section falls significantly below the total configuration-average distorted-wave direct ionization cross section, though is in good agreement above about 300 eV.

B. Bi^{2+}

The theoretical and experimental results for Bi^{2+} are shown in Fig. 2. Bi^{2+} has a ground configuration of $5d^{10}6s^26p$. Again, the current experimental measurements are in good agreement with the previous measurements of Müller *et al.* [15]. Direct ionization from the 6*s*, 6*p*, and 5*d* subshells is included, as well as excitation-autoionization

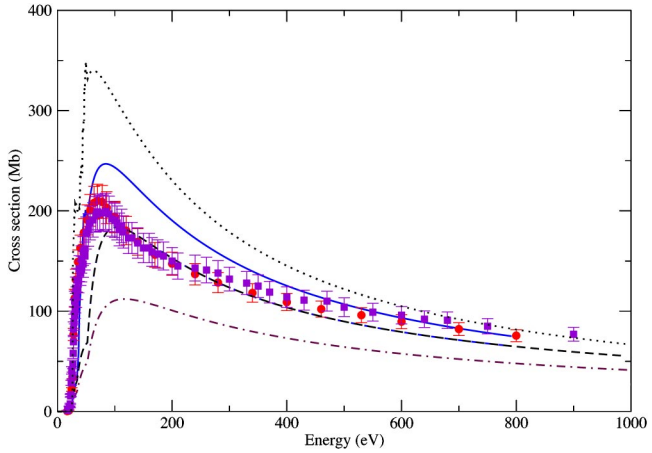

FIG. 2. Electron-impact single ionization cross section for Bi^{2+}. The dashed line gives the total configuration-average distorted-wave direct ionization; the dotted line gives the total of the configuration-average distorted-wave direct ionization plus the configuration-average distorted-wave excitation-autoionization. The solid line gives the statistically partitioned configuration-average distorted-wave results. The dot-dashed line shows the Lotz direct ionization cross section. The solid circles show the current experimental measurements and the solid squares show the measurements of Müller *et al.* [15].

TABLE II. Configuration-average ionization potentials for the subshells in the ground configuration of Bi^{2+}; the configuration-average double ionization potential is 67.30 eV.

Transition	Configuration-average ionization potential (eV)
$5d^{10}6s^26p \rightarrow 5d^{10}6s^2$	23.84
$5d^{10}6s^26p \rightarrow 5d^{10}6s6p$	34.55
$5d^{10}6s^26p \rightarrow 5d^96s^26p$	52.26

via the $5d^96s^26pnl$ and $5d^{10}6s^16pnl$ configurations, where $n=5-8$ and $l=0-3$. It can be seen that the basic configuration-average distorted-wave result lies significantly higher than experiment. Some of the autoionizing configurations lie close to the ionization threshold, in particular the $5d^96s^26p^2$ configuration, with a configuration-average energy of 26.8 eV, compared to the configuration-average ionization threshold of 23.84 eV. In the case of Bi^{2+}, the terms and level splitting within the excited configurations are causing the levels to straddle the autoionization threshold. We used the AUTOSTRUCTURE code [17] to evaluate level energies and Auger yields, which were then used to adjust configuration-average excitation cross sections. The main adjustment to the statistically partitioned cross section comes via the adjustment to the $5d^96s^26p^2$ configuration. Excitation to the $5d^96s^26p^2$ configuration is the largest contribution to the excitation-autoionization cross section; thus the partitioning of this configuration produces the most significant reduction in the total theoretical cross section. The remaining excited configurations associated with core excitation of the $5d$ subshell all make a small contribution to the total excitation-autoionization cross section. Partitioning of these configurations produces a further small reduction in the total cross section. It can be seen from Fig. 2 that the statistically partitioned results lie in closer agreement with experiment, although they still slightly overestimate the peak of the cross section. It is also to be noted that the DWIS($N-1$) results for the direct ionization lie slightly lower than the DWIS(N) results. For all other ion stages which were investigated the DWIS($N-1$) results were almost identical to the DWIS(N) results, and we show only the DWIS($N-1$) results. Table II shows the direct ionization potentials for Bi^{2+}. The total Lotz cross section falls significantly below the configuration-average distorted-wave direct ionization cross section at all energies. This difference is largely due to differences in the $5d$ direct ionization cross section.

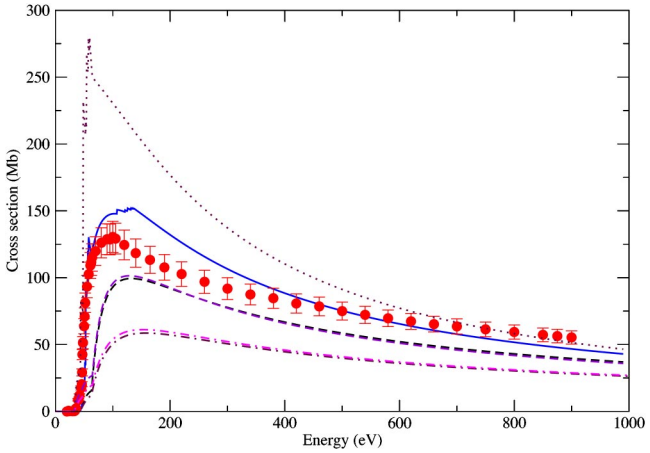

FIG. 3. Electron-impact single ionization cross section for Bi^{3+}. The dashed line shows the ground state direct ionization; the solid line shows the ground state direct ionization plus the excitation-autoionization cross section. The two dashed lines show the excited configuration total direct ionization (upper curve shows the excited configuration results while the lower curve shows the ground configuration results). The dotted line shows the direct plus excitation-autoionization cross section for excited configuration ionization. The two dot-dashed lines shows the Lotz direct ionization cross section, with the upper curve giving the first excited configuration ionization cross section, and the lower curve showing the ground configuration results. The solid circles show the experimental results.

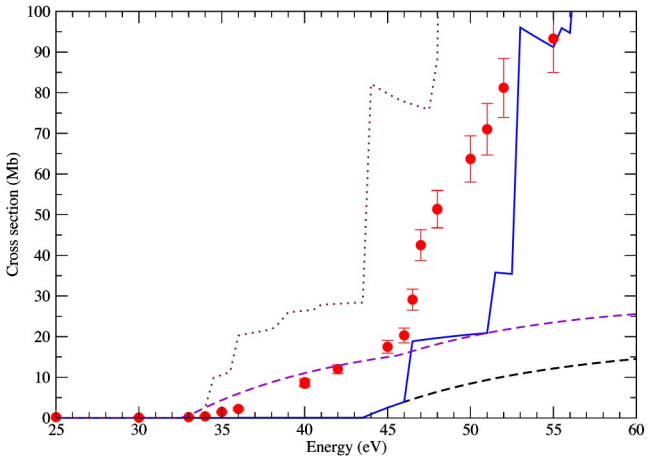

FIG. 4. Electron-impact single ionization cross section for Bi^{3+} in the near threshold region. The lower dashed line shows the ground state direct ionization; the solid line shows the ground state direct ionization plus the excitation-autoionization cross section. The upper dashed line shows the excited configuration total direct ionization, and the dotted line shows the direct plus excitation-autoionization cross section for excited configuration ionization. The solid circles show the experimental results.

C. Bi^{3+}

The theoretical and experimental results for Bi^{3+} are shown in Fig. 3. Bi^{3+} has a ground configuration of $5d^{10}6s^2$. We show the configuration-average distorted-wave results

TABLE III. Configuration-average ionization potentials for the subshells in the ground configuration of Bi^{3+}; the configuration-average double ionization potential is 98.52 eV.

Transition	Configuration-average ionization potential (eV)
$5p^65d^{10}6s^2 \rightarrow 5p^65d^{10}6s$	43.46
$5p^65d^{10}6s^2 \rightarrow 5p^65d^96s^2$	62.95
$5p^65d^{10}6s^2 \rightarrow 5p^55d^{10}6s^2$	141.90

TABLE IV. Configuration-average ionization potentials for the subshells in the first excited configuration of Bi^{3+}; the configuration-average double ionization potential is 98.52 eV.

Transition	Configuration-average ionization potential (eV)
$5p^6 5d^{10} 6s6p \rightarrow 5p^6 5d^{10} 6s$	32.74
$5p^6 5d^{10} 6s6p \rightarrow 5p^6 5d^{10} 6p$	45.69
$5p^6 5d^{10} 6s6p \rightarrow 5p^6 5d^9 6s6p$	64.43
$5p^6 5d^{10} 6s6p \rightarrow 5p^5 5d^{10} 6s6p$	143.55

assuming both a 100% $5d^{10}6s^2$ ground state, and a 100% $5d^{10}6s6p$ excited configuration. For the ground configuration we include direct ionization from the 6*s* and 5*d* subshells. We include indirect ionization via core excitation of a 5*d* and 5*p* subshell for the ground configuration. As can be seen from Fig. 3 there is reasonable agreement with the experimental cross section. Closer inspection of the threshold region (see Fig. 4) shows that there is a significant metastable fraction below the ground ionization threshold. This threshold agrees well with the ionization threshold of the first excited configuration. For the first excited configuration we include direct ionization of the 6*p*, 6*s*, and 5*d* subshells and indirect ionization via core excitation of the 6*s* and 5*d* subshells. Tables III and IV show the direct ionization potentials for the ground and first excited configurations of Bi^{3+}. The metastable cross section significantly overestimates the total cross section, indicating that the metastable fraction may be small. To match the cross section in the region below the ground ionization threshold requires approximately 30% metastable fraction. The total Lotz cross section lies significantly below the configuration-average distorted-wave direct ionization results.

D. Bi^{4+}

The theoretical and experimental results for Bi^{4+} are shown in Fig. 5. Bi^{4+} has a ground configuration of $5d^{10}6s$.

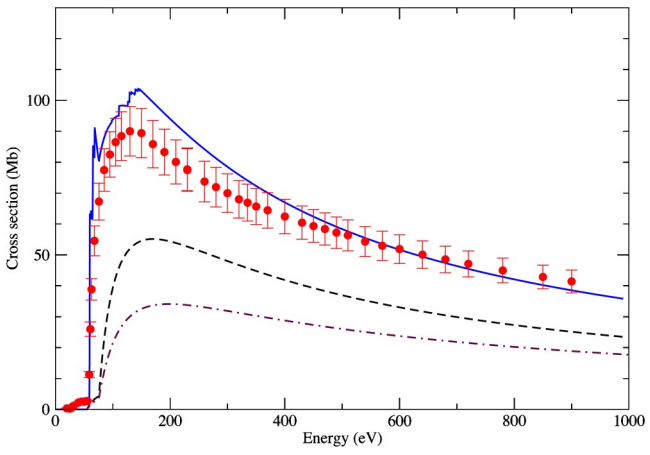

FIG. 5. Electron-impact single ionization cross section for Bi^{4+}. The dashed line shows the total direct ionization cross section, the solid line shows the total direct plus the total excitation-autoionization cross section, the dot-dashed line shows the total Lotz direct ionization cross section, and the solid circles show the experimental results.

TABLE V. Configuration-average ionization potentials for the subshells in the ground configuration of Bi^{4+}; the configuration-average double ionization potential is 144.21 eV.

Transition	Configuration-average ionization potential (eV)
$5p^6 5d^{10} 6s \rightarrow 5p^6 5d^{10}$	55.06
$5p^6 5d^{10} 6s \rightarrow 5p^6 5d^9 6s$	75.76
$5p^6 5d^{10} 6s \rightarrow 5p^5 5d^{10} 6s$	155.08

With a ground state of $5s^2 5d^{10}6s$, we do not expect to have significant metastable fraction. There is a small amount of cross section below the theoretical ionization threshold. We include direct ionization of the 6*s* and 5*d* subshells. Note that ionization of the 5*p* subshell lies above the double ionization threshold with a configuration-averaged ionization potential of 155 eV, compared to the double ionization potential of 144 eV. Table V shows the direct ionization potentials for Bi^{4+}. The theory agrees well with the onset of the excitation-autoionization cross section, and although slightly higher than experiment at the peak of the cross section, is in broad agreement above the peak. Again, the total Lotz ionization cross section lies significantly below the total direct ionization from the configuration-average distorted-wave results.

E. Bi^{5+}

The theoretical and experimental results for Bi^{5+} are shown in Fig. 6. Bi^{5+} has a ground configuration of $5d^{10}$. The

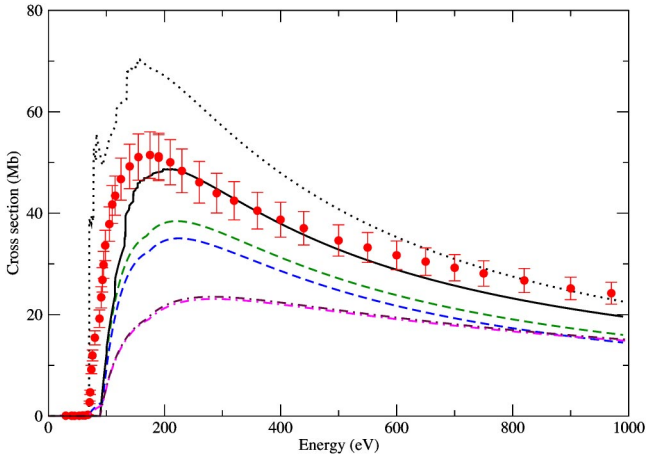

FIG. 6. Electron-impact single ionization cross section for Bi^{5+}. The lower dashed line shows the direct ionization cross section for the ground configuration while the solid line gives the total direct ionization plus the total excitation-autoionization cross section for the ground configuration. The upper dashed curve gives the total direct ionization for the first excited configuration, and the dotted curve configuration gives the total direct ionization plus the excitation-autoionization cross section for the excited configuration. The two dot-dashed curves show the total Lotz direct ionization cross sections results, with the upper curve showing the excited configuration results, and the lower curve showing the ground configuration results. The solid circles show the experimental results.

TABLE VI. Configuration-average ionization potentials for the subshells in the ground configuration of Bi^{5+}; the configuration-average double ionization potential is 196.32 eV.

Transition	Configuration-average ionization potential (eV)
$4f^{14}5s^25p^65d^{10} \rightarrow 4f^{14}5s^25p^65d^9$	89.15
$4f^{14}5s^25p^65d^{10} \rightarrow 4f^{14}5s^25p^55d^{10}$	168.87
$4f^{14}5s^25p^65d^{10} \rightarrow 4f^{14}5s5p^65d^{10}$	233.65
$4f^{14}5s^25p^65d^{10} \rightarrow 4f^{13}5s^25p^65d^{10}$	224.97

experimental ionization threshold is in good agreement with the ionization threshold for the first excited configuration, $5d^96s$. For the ground configuration we include direct ionization from the $5d$ and $5p$ subshells and excitation-autoionization via core excitation of the $5s$, and $5p$ subshells. For the first excited configuration we include direct ionization of the $6s$, $5d$, and $5p$ subshells, and excitation-autoionization via core excitation of the $5p$ and $5d$ subshells. Tables VI and VII shows the direct ionization potentials for Bi^{5+}. It can be seen that the excitation-autoionization contribution from the first excited configuration results in a cross section greater than that of experiment, while the ground configuration ionization cross section is slightly lower than experiment. The large amount of cross section in the region below the ground ionization potential indicates a large excited configuration fraction in the beam. The total Lotz ionization cross section lies significantly below the configuration-average distorted-wave results until about 800 eV, when there is reasonable agreement.

F. Bi^{6+}

The theoretical and experimental results for Bi^{6+} are shown in Fig. 7. Bi^{6+} has a ground configuration of $5d^9$. We include direct ionization of the $5d$ and $5p$ subshells and excitation-autoionization via core excitation of the $5p$ and $5s$ subshells. Table VIII shows the direct ionization potentials for Bi^{6+}. There is clearly significant excitation-autoionization, with distorted-wave theory giving a good match to experiment.

Bi^{6+} shows some evidence of below threshold ionization, suggesting that there is perhaps some metastable presence, or that the term-resolved direct ionization threshold is somewhat lower than the configuration-average threshold ionization potential. The total Lotz ionization cross section lies

TABLE VII. Configuration-average ionization potentials for the subshells in the first excited configuration of Bi^{5+}; the configuration-average double ionization potential is 196.32 eV.

Transition	Configuration-average ionization potential (eV)
$4f^{14}5s^25p^65d^96s \rightarrow 4f^{14}5s^25p^65d^9$	68.46
$4f^{14}5s^25p^65d^96s \rightarrow 4f^{14}5s^25p^65d^86s$	93.15
$4f^{14}5s^25p^65d^96s \rightarrow 4f^{14}5s^25p^55d^96s$	173.03

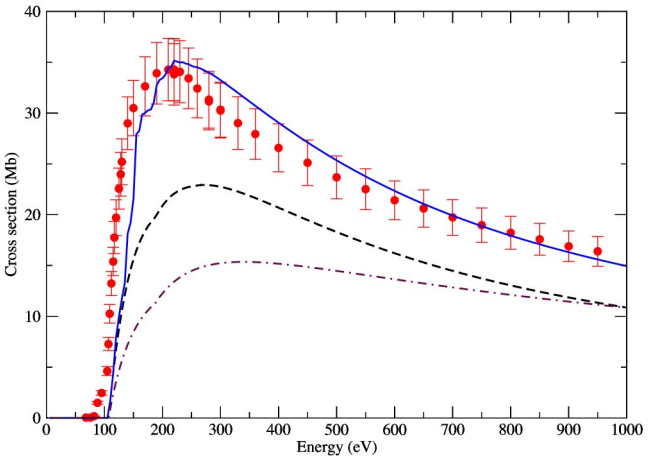

FIG. 7. Electron-impact single ionization cross section for Bi^{6+}. The dashed line shows the total direct ionization cross section, the solid line shows the total direct plus the excitation-autoionization cross section, the dot-dashed curve shows the Lotz total direct ionization cross section, and the solid circles show the experimental results.

significantly below the configuration-average distorted-wave results until about 900 eV, when there is good agreement.

G. Bi^{7+}

The theoretical and experimental results for Bi^{7+} are shown in Fig. 8. Bi^{7+} has a ground configuration of $5d^8$. We include direct ionization of the $5d$, $5p$, and $4f$ subshells, and excitation-autoionization via core excitation of the $5p$ and $5s$ subshells. Table IX shows the direct ionization potentials for Bi^{7+}. Again, there is reasonably good agreement between theory and experiment. Once one enters significantly into the $5d$ subshell, one would expect the configuration-average distorted-wave calculations to be in closer agreement with experiment. This is because of the large number of terms associated with an open $5d$ subshell, so any metastable terms present are likely to be contained within the ground configuration. Thus, the configuration-average ionization result for the lowest configuration should contain the effects of any metastable presence as well. The total Lotz ionization cross section lies below the configuration-average distorted-wave results until about 800 eV, when there is good agreement.

H. Bi^{8+}

The theoretical and experimental results for Bi^{8+} are shown in Fig. 9. Bi^{8+} has a ground configuration of $5d^7$. We include direct ionization of the $5d$, $5p$, $5s$, and $4f$ subshells,

TABLE VIII. Configuration-average ionization potentials for the subshells in the ground configuration of Bi^{6+};the configuration-average double ionization potential is 232.99 eV.

Transition	Configuration-average ionization potential (eV)
$4f^{14}5s^25p^65d^9 \rightarrow 4f^{14}5s^25p^65d^8$	107.16
$4f^{14}5s^25p^65d^9 \rightarrow 4f^{14}5s^25p^55d^9$	187.46
$4f^{14}5s^25p^65d^9 \rightarrow 4f^{14}5s5p^65d^9$	253.09

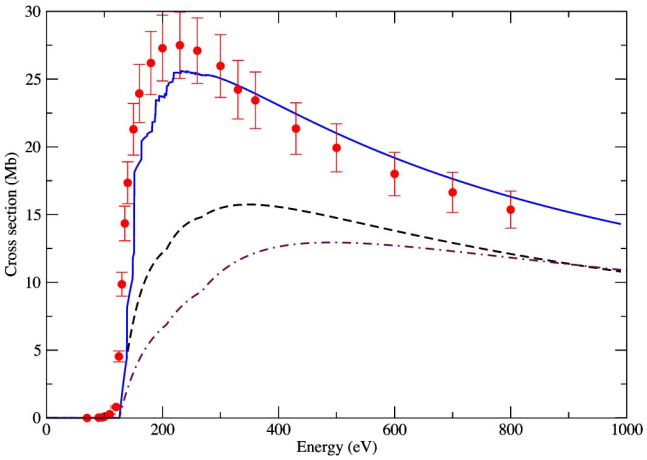

FIG. 8. Electron-impact single ionization cross section for Bi^{7+}. The dashed line shows the total direct ionization cross section, the solid line shows the total direct plus excitation-autoionization cross section, the dot-dashed curve shows the Lotz total direct ionization cross section, and the solid circles show the experimental results.

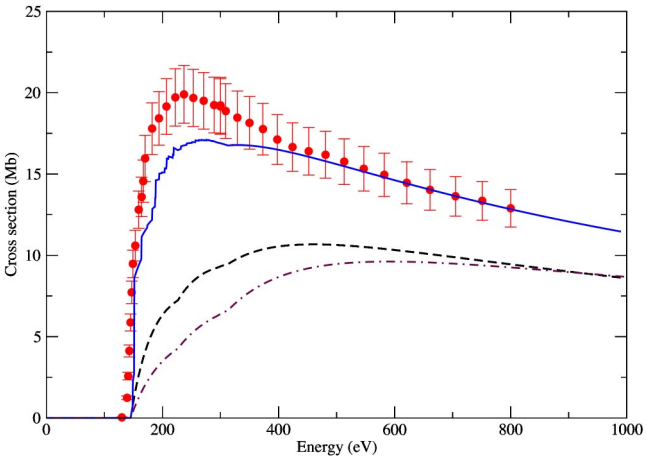

FIG. 9. Electron-impact single ionization cross section for Bi^{8+}. The dashed line shows the total direct ionization cross section, the solid line shows the total direct plus excitation-autoionization cross section, the dot-dashed curve shows the Lotz total direct ionization cross section, and the solid circles show the experimental results.

and excitation-autoionization via core excitation of the $5p$ and $5s$ subshells. Table X shows the direct ionization potentials for Bi^{8+}. The results for Bi^{8+} lie slightly below those of experiment at the peak of the cross section, but agree well at higher energy. It should be noted that direct ionization of the $4f$ subshell lies very close to the double ionization potential for Bi^{8+}, and in the configuration-average picture actually lies slightly above, suggesting that it should all double ionize. However, inclusion of direct ionization of the $4f$ subshell provides much better agreement with experiment at high energy, suggesting that term and level splitting is causing the majority of the direct ionization to fall in the single ionization regime or that there is a significant radiative branching ratio of the ionized configuration. A level-resolved AUTOSTRUCTURE calculation reveals that the $4f$ ionization does indeed lie below the double ionization threshold. The total Lotz ionization cross section lies below the configuration-average distorted-wave results until about 800 eV, when there is good agreement.

I. Bi^{9+}

The theoretical and experimental results for Bi^{9+} are shown in Fig. 10. Bi^{9+} has a ground configuration of $5d^6$. In the theoretical calculations we include direct ionization from

TABLE IX. Configuration-average ionization potentials for the subshells in the ground configuration of Bi^{7+}; the configuration-average double ionization potential is 270.95 eV.

Transition	Configuration-average ionization potential (eV)
$4f^{14}5s^25p^65d^8 \rightarrow 4f^{14}5s^25p^65d^7$	125.83
$4f^{14}5s^25p^65d^8 \rightarrow 4f^{14}5s^25p^55d^8$	206.70
$4f^{14}5s^25p^65d^8 \rightarrow 4f^{14}5s5p^65d^8$	273.22
$4f^{14}5s^25p^65d^8 \rightarrow 4f^{13}5s^25p^65d^8$	267.33

TABLE X. Configuration-average ionization potentials for the subshells in the ground configuration of Bi^{8+}; the configuration-average double ionization potential is 310.11 eV.

Transition	Configuration-average ionization potential (eV)
$4f^{14}5s^25p^65d^7 \rightarrow 4f^{14}5s^25p^65d^6$	145.12
$4f^{14}5s^25p^65d^7 \rightarrow 4f^{14}5s^25p^55d^7$	226.54
$4f^{14}5s^25p^65d^7 \rightarrow 4f^{14}5s5p^65d^7$	294.00
$4f^{14}5s^25p^65d^7 \rightarrow 4f^{13}5s^25p^65d^7$	313.08

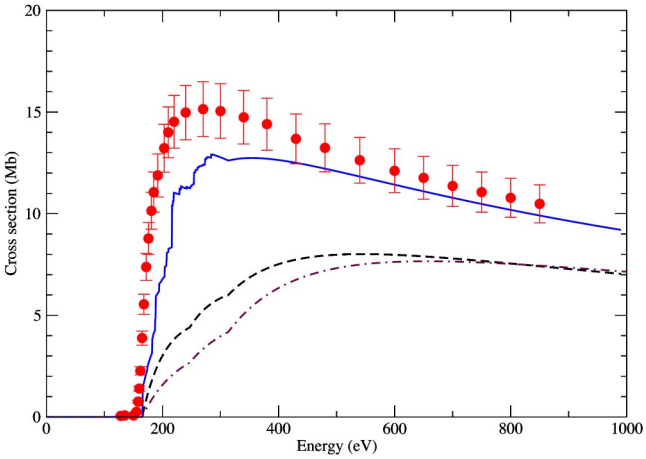

FIG. 10. Electron-impact single ionization cross section for Bi^{9+}. The dashed line shows the total direct ionization cross section, the solid line shows the total direct plus excitation-autoionization cross section, the dot-dashed curve shows the Lotz total direct ionization cross section, and the solid circles show the experimental results.

TABLE XI. Configuration-average ionization potentials for the subshells in the ground configuration of Bi^{9+}; the configuration-average double ionization potential is 350.43 eV.

Transition	Configuration-average ionization potential (eV)
$4f^{14}5s^25p^65d^6 \rightarrow 4f^{14}5s^25p^65d^5$	164.99
$4f^{14}5s^25p^65d^6 \rightarrow 4f^{14}5s^25p^55d^6$	246.93
$4f^{14}5s^25p^65d^6 \rightarrow 4f^{14}5s5p^65d^6$	315.38
$4f^{14}5s^25p^65d^6 \rightarrow 4f^{13}5s^25p^65d^6$	313.08

TABLE XII. Configuration-average ionization potentials for the subshells in the ground configuration of Bi^{10+}; the configuration-average double ionization potential is 391.85 eV.

Transition	Configuration-average ionization potential (eV)
$4f^{14}5s^25p^65d^5 \rightarrow 4f^{14}5s^25p^65d^4$	185.44
$4f^{14}5s^25p^65d^5 \rightarrow 4f^{14}5s^25p^55d^5$	267.87
$4f^{14}5s^25p^65d^5 \rightarrow 4f^{14}5s5p^65d^5$	337.34
$4f^{14}5s^25p^65d^5 \rightarrow 4f^{13}5s^25p^65d^5$	337.12

the $5d$, $5p$, $5s$, and $4f$ subshells, and excitation-autoionization from core excitations of the $5p$, $5s$, and $4f$ subshells. Table XI shows the direct ionization potentials for Bi^{9+}. It can be seen that the $5s$ and the $4f$ subshells fall just inside the single ionization region. The theory is in reasonable agreement with experiment, except at the peak of the cross section, where theory comes in lower than experiment. The total Lotz ionization cross section is a little lower than the configuration-average distorted-wave results, and by 700 eV is in good agreement.

J. Bi^{10+}

The theoretical and experimental results for Bi^{10+} are shown in Fig. 11. Bi^{10+} has a ground configuration of $5d^5$. In the theory results we include direct ionization from the $5d$, $5p$, $5s$, and $4f$ subshells and excitation-autoionization via core excitation of the $5p$, $5s$, and $4f$ subshells. Table XII shows the direct ionization potentials for Bi^{10+}. It can be seen that the $5s$ and the $4f$ subshells fall within the single ionization region. As can be seen from Fig. 11, there is reasonable agreement between theory and experiment, though again theory is slightly lower than experiment at the peak of the cross section. The total Lotz ionization cross section is slightly lower than the configuration-average distorted-wave direct ionization results, and by 700 eV is in good agreement. It should, however, be noted that the Lotz expression does not account for excitation-autoionization, and thus is still significantly lower than experiment.

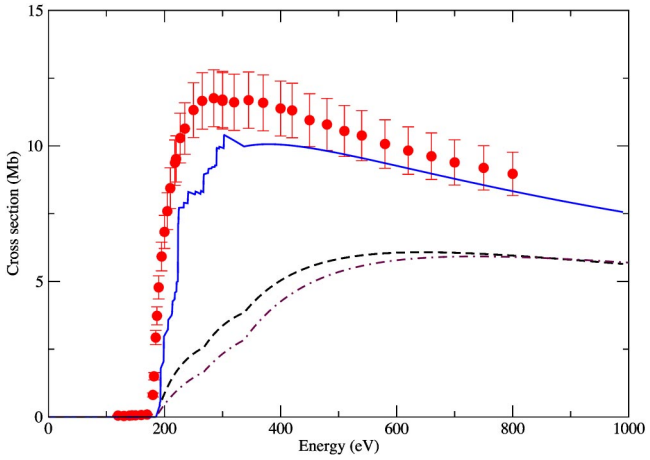

FIG. 11. Electron-impact single ionization cross section for Bi^{10+}. The dashed line shows the total direct ionization cross section, the solid line shows the total direct plus excitation-autoionization cross section, the dot-dashed curve shows the Lotz total direct ionization cross section, and the solid circles show the experimental results.

V. SUMMARY

Recent experimental measurements for electron-impact single ionization of Bi^+ through to Bi^{10+} have been compared with configuration-average distorted-wave theory. Good agreement is obtained for most of the ion stages. For Bi^{2+} account was taken of level splitting of the autoionizing configurations. The contribution to the measured cross section from excited configurations, containing metastable terms, was found to be significant for Bi^{3+} and Bi^{5+}. There is, in general, good agreement between configuration-average distorted-wave results, and those of experiment. The Lotz ionization cross section results become a reasonable approximation to the direct ionization cross sections as the charge state increases, although they are still significantly below the experimental measurements due to the large amount of excitation-autoionization present in the total cross section.

ACKNOWLEDGMENTS

This work was supported by a grant for Scientific Discovery through Advanced Computing by the U.S. Department of Energy. Support by the Deutsche Forschungsgemeinschaft (DFG), Bonn-Bad Godesberg, is gratefully acknowledged.

[1] ITER Physics Basis Editors, ITER Physics Expert Group Chairs and Co-Chairs, and ITER Joint Central Team and Physics Integration Unit, Nucl. Fusion **39**, 2137 (1999).
[2] H. P. Summers, N. R. Badnell, M. G. O'Mullane, A. D. Whiteford, R. Bingham, B. J. Kellett, J. Lang, K. H. Behringer, U. Fantz, K-D. Zastrow, S. D. Loch, M. S. Pindzola, D. C. Griffin, and C. P. Ballance, Plasma Phys. Controlled Fusion **44**, B323 (2002).
[3] M.S. Pindzola, D.C. Griffin, and C. Bottcher, in *Atomic Processes in Electron-Ion and Ion-Ion Collisions*, NATO Advanced Study Institute, Series B: Physics, edited by F. Brouillard (Plenum, New York, 1986), Vol. 145.
[4] M.S. Pindzola, D.C. Griffin, and C. Bottcher, Phys. Rev. A **34**, 3668 (1986).
[5] M.S. Pindzola, D.C. Griffin, C. Bottcher, S.M. Younger, and T.H. Hunter, Nucl. Fusion Suppl. **1**, 21 (1987).
[6] M.S. Pindzola and D.C. Griffin, J. Phys. B **21**, 3253 (1988).
[7] M.S. Pindzola, D.C. Griffin, C. Bottcher, M.J. Buie, and D.C. Gregory, Phys. Scr., T **37**, 35 (1991).
[8] J.A. Shaw, M.S. Pindzola, M. Steidl, K. Aichele, U. Hartenfeller, D. Hathiramani, F. Scheuermann, M. Westermann, and E. Salzborn, Phys. Rev. A **63**, 032709 (2001).
[9] D. Hathiramani, K. Aichele, G. Hofmann, M. Steidl, M. Stenke, R. Völpel, E. Salzborn, M.S. Pindzola, J.A. Shaw, D.C. Griffin, and N.R. Badnell, Phys. Rev. A **54**, 587 (1996).
[10] K. Aichele, W. Arnold, D. Hathiramani, F. Scheuermann, E. Salzborn, D.M. Mitnik, D.C. Griffin, J. Colgan, and M.S. Pindzola, Phys. Rev. A **64**, 052706 (2001).
[11] M. Stenke, K. Aichele, D. Hathiramani, G. Hofmann, M. Steidl, R. Völpel, and E. Salzborn, J. Phys. B **28**, 2711 (1995).
[12] M.S. Pindzola and D.C. Griffin, Phys. Rev. A **56**, 1654 (1997).
[13] S.D. Loch, M.S. Pindzola, C.P. Ballance, D.C. Griffin, D.M. Mitnik, N.R. Badnell, M.G. O'Mullane, H.P. Summers, and A.D. Whiteford, Phys. Rev. A **66**, 052708 (2002).
[14] S.D. Loch, A.D. Whiteford, and M.S. Pindzola (private communication).
[15] A. Müller, K. Tinschert, Ch. Achenbach, E. Salzborn, R. Becker, and M.S. Pindzola, Phys. Rev. Lett. **54**, 414 (1985).
[16] W. Lotz, Z. Phys. **216**, 241 (1968).
[17] N.R. Badnell, J. Phys. B **19**, 3827 (1986).
[18] N.R. Badnell, J. Phys. B **30**, 1 (1997).
[19] N.R. Badnell and M.S. Pindzola, Phys. Rev. A **39**, 1685 (1989).
[20] K. Tinschert, A. Müller, G. Hofmann, K. Huber, R. Becker, D.C. Gregory, and E. Salzborn, J. Phys. B **22**, 531 (1989).
[21] G. Hofmann, A. Müller, K. Tinschert, and E. Salzborn, Z. Phys. D: At., Mol. Clusters **16**, 113 (1990).
[22] F. Brötz, dissertation, University of Giessen, 2000, http://geb.uni-giessen.de/geb/volltexte/2000/263/
[23] R. Becker, A. Müller, Ch. Achenbach, K. Tinschert, and E. Salzborn, Nucl. Instrum. Methods Phys. Res. B **9**, 385 (1985).